## SUPPLEMENTARY INFORMATION

# Epitranscriptomic $m^6A$ Regulation of Axon Regeneration in the Adult Mammalian Nervous System

Yi-Lan Weng, Xu Wang, Ran An, Jessica Cassin, Caroline Vissers, Yuanyuan Liu, Yajing Liu, Tianlei Xu, Xinyuan Wang, Samuel Zheng Hao Wong, Jessica Joseph, Louis C. Dore, Qian Dong, Wei Zheng, Peng Jin, Hao Wu, Bin Shen, Xiaoxi Zhuang, Chuan He, Kai Liu, Hongjun Song and Guo-li Ming

## INVENTORY

**Supplementary Figures 1-6**

## SUPPLEMENTARY FIGURES

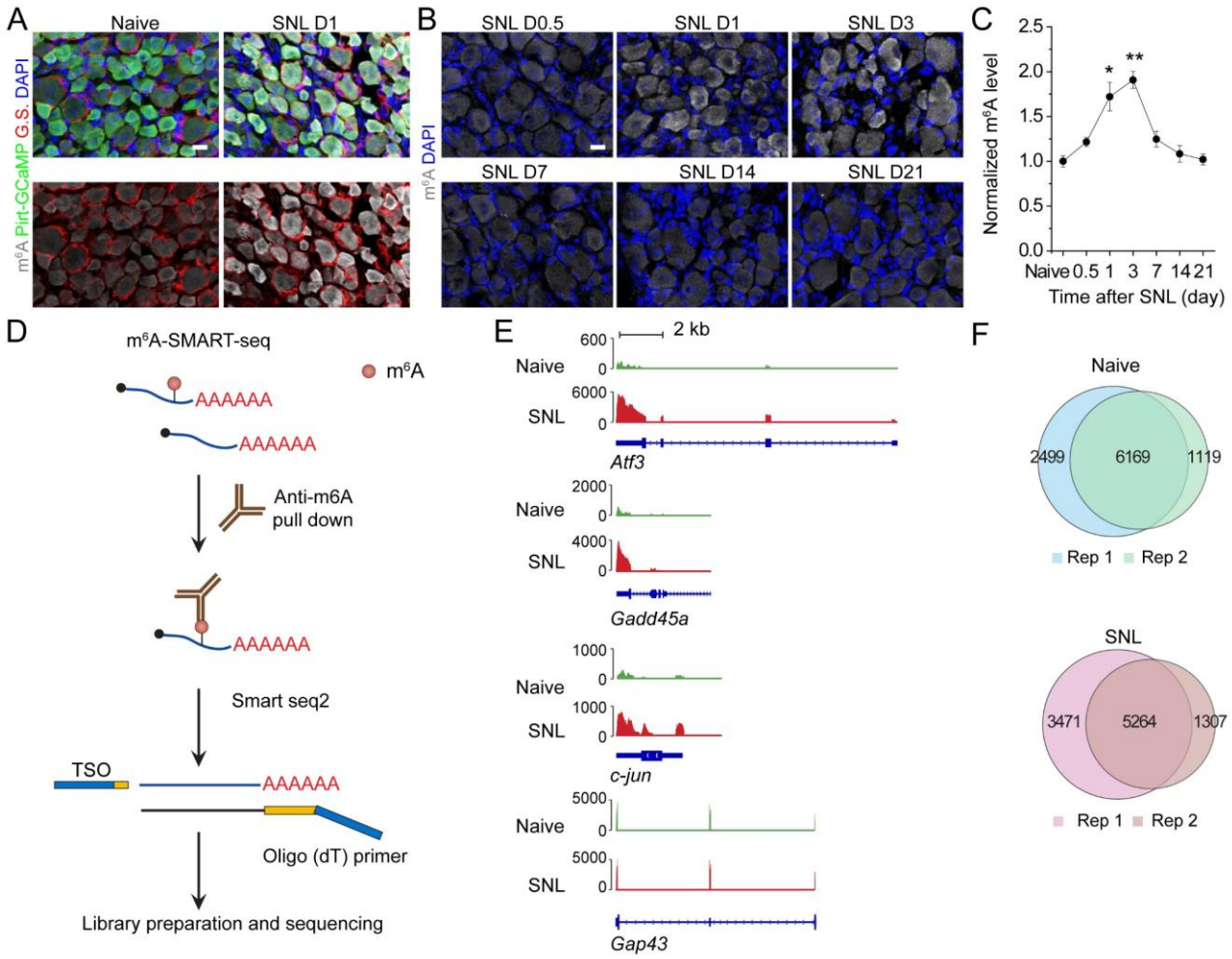


**Figure S1. m$^6$A immunohistology and m$^6$A-SMART-seq analysis of m$^6$A-tagged transcript levels in the adult mouse DRGs under naïve and SNL conditions, related to Figure 1.**
(**A**) Sample images of adult DRGs from neuronal reporter *Pirt-GCaMP3* mice immunostained for GFP and glutamine synthetase (G.S.), a satellite glia marker, under naïve and SNL D1 conditions. Scale bar: 20 μm.
(**B-C**) Time course analysis of m$^6$A levels in adult DRGs upon injury. Shown are sample images for m$^6$A immunostaining (**B;** scale bar: 20 μm) and quantification (**C**). Values represent mean ± SEM (n = 3 animals; ***P* < 0.01; **P* < 0.05; two-way ANOVA).
(**D**) A schematic diagram of the m$^6$A-SMART-seq protocol. TSO, Template-Switching Oligo.
(**E**) UCSC genome browser tracks of m$^6$A-SMART-seq showing representative examples of m$^6$A transcript levels changes after injury for a selective group of RAGs, including *Atf3*, *Gadd45a*, *c-jun* and *Gap43*.
(**F**) Venn diagrams showing the overlap of m$^6$A-tagged transcripts between two replicates in naïve and SNL D1 DRGs.

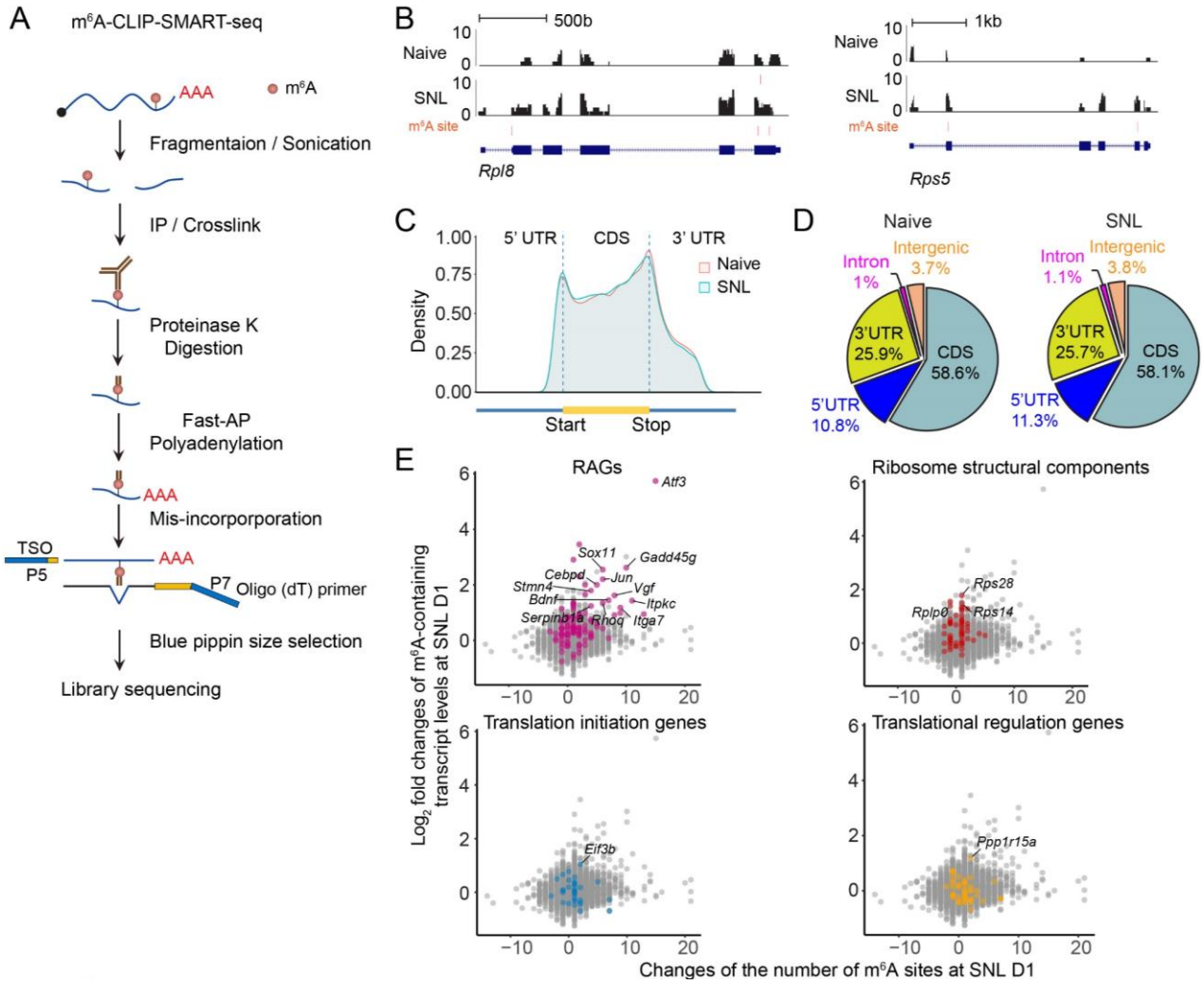


**Figure S2. m$^6$A-CLIP-SMART-seq analysis of m$^6$A sites in adult mouse DRGs under naïve and SNL D1 conditions, related to Figure 2.**

(**A**) A schematic diagram of the m$^6$A-CLIP-SMART-seq protocol.

(**B**) UCSC genome browser tracks of m$^6$A-CLIP-SMART-seq showing representative examples of m$^6$A site changes after injury for two ribosomal subunit-related genes.

(**C**) Metagene profiles showing the m$^6$A site density distribution across the transcriptome of DRGs under naïve and SNL D1 conditions.

(**D**) Pie charts depicting fractions of m$^6$A sites in different transcript segments. UTR: untranslated region; CDS: coding sequence region.

(**E**) Scatter plots of $\log_2$ fold changes of m$^6$A-containing transcript levels (from m$^6$A-SMART-seq) and changes in the number of m$^6$A sites (from m$^6$A-CLIP-seq) under naïve and SNL D1 conditions. Subsets of genes are labeled with different colors as in **Figure 1G**: RAGs (magenta), ribosomal subunit-related genes (red), translation initiation-related genes (blue), and translation regulation-related genes (yellow).

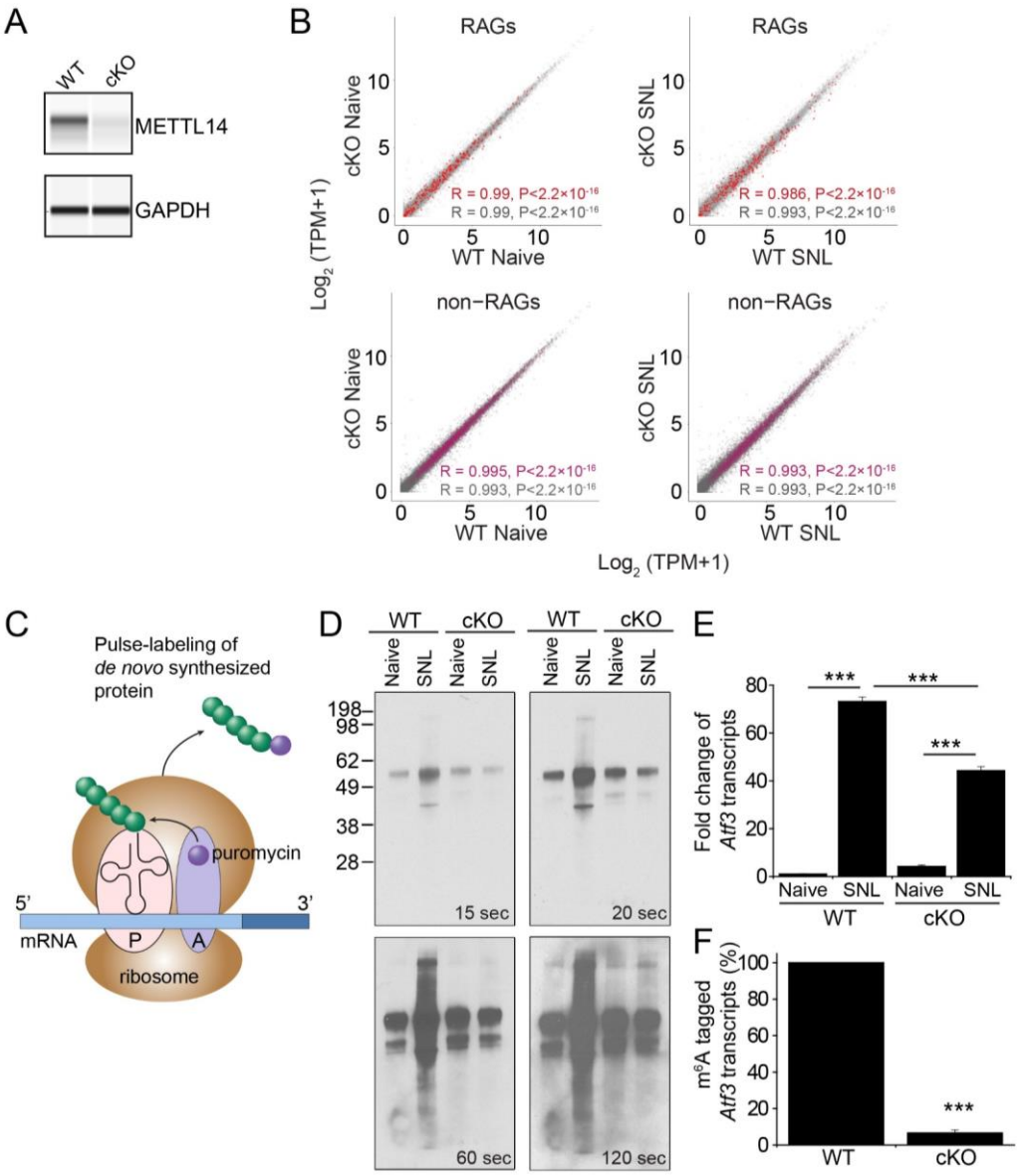


**Figure S3. *Mettl14* deletion diminishes m$^6$A levels in mRNA, but has minimal impact on the transcriptomes of DRGs under naïve and SNL conditions, related to Figure 3.**

(**A**) Sample western blot analysis of Mettl14 expression in DRGs from adult WT and *Syn1-Cre;Mettl14$^{f/f}$* cKO mice. GAPDH is shown as the loading control.

(**B**) Scatter plot showing the correlation of gene expression levels of all transcripts in RNA-seq of WT and *Mettl14* cKO DRGs under naïve conditions and at SNL D1. RAGs are indicated by red dots and non-RAGs are indicated by magenta dots. The Pearson correlation coefficient and *P* value are indicated.

(**C**) A schematic diagram of SUnSET assay.

(**D**) SUnSET analysis of new protein synthesis in L4/5 DRGs of adult WT and *Mettl14* cKO mice. Same sample as in **Figure 3C**, but with different exposures.

(**E**) *Atf3* mRNA levels in WT and *Mettl14* cKO DRGs under naïve and SNL D1 conditions. Values represent mean ± SEM (n = 3 animals; ***$P$ < 0.01; two-way ANOVA).

(**F**) m$^6$A-tagged transcript levels in WT and *Mettl14* cKO DRGs at SNL D1. Values represent mean ± SEM (n = 3 animals; ***$P$ < 0.01; two-way ANOVA).

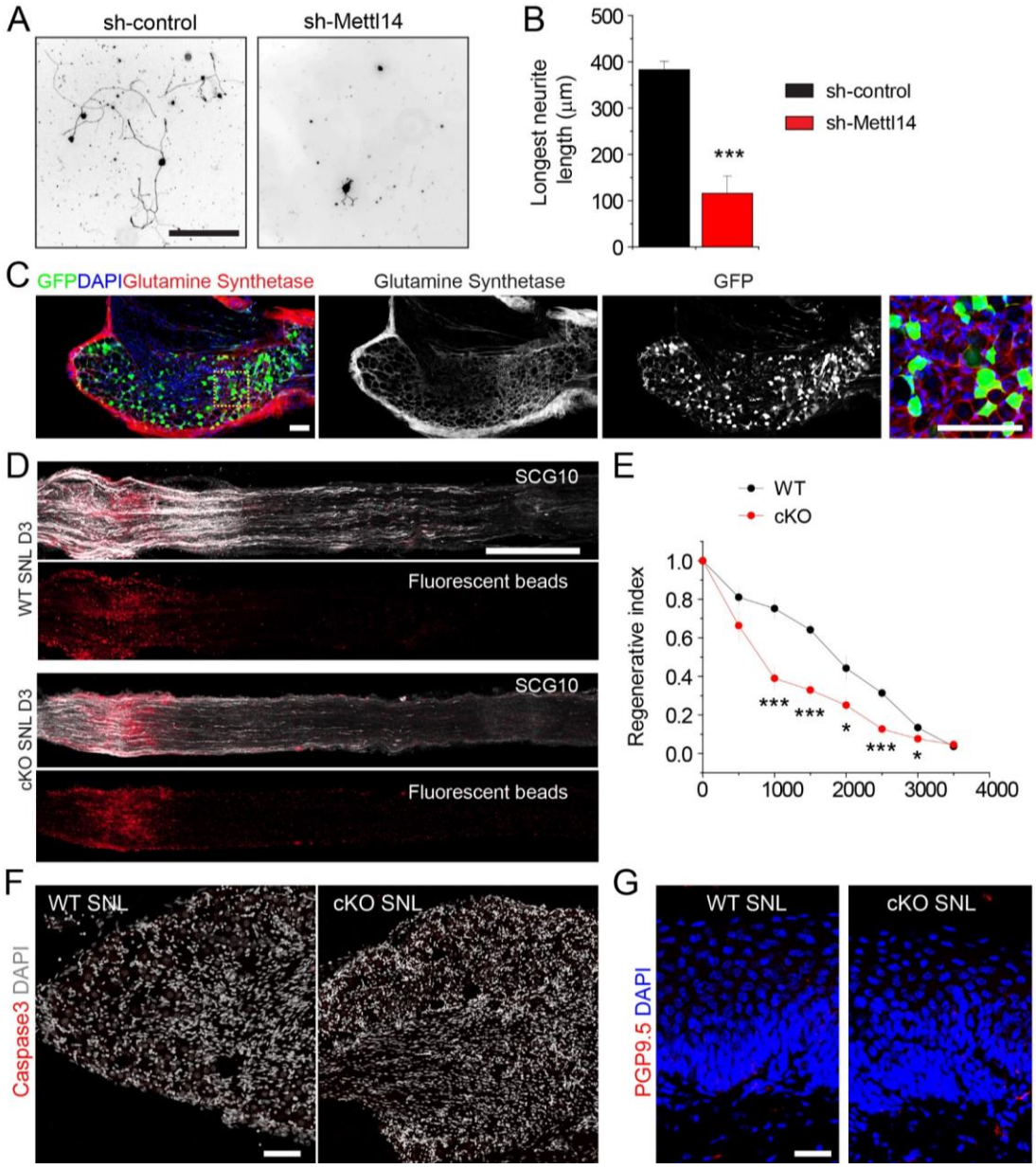


**Figure S4. Effects of *Mettl14* deletion on DRG neuron survival and regeneration upon SNL, related to Figure 4.**

(**A-B**) In vitro analysis of DRG neuron axon regeneration. Adult DRG neurons were dissociated and cultured with AAV-control shRNA or AAV-Mettl14 shRNA for 10 days. Neurons were then replated and fixed 24 h after replating. DRG neurites were visualized by Tuj1 staining. Shown in (**A**) are sample images of replated neurons with Tuj1 staining under different conditions. Scale bar: 400 μm. Shown in (**B**) are summaries for quantifications of the length of the longest axon for each DRG neuron. Values represent mean ± SEM (n = 3 experimental replications; **P* < 0.05; Student's t-test).

(**C**) Sample images of DRGs infected with AAV2/9 to express GFP. Shown are sample images for immunostaining of glutamine synthetase, a marker for satellite glia in DRGs. Note that AAV2/9 shows limited tropism toward satellite glia. Scale bars: 100 μm.

(**D-E**) Sample images of regenerating sensory axons identified by SCG10 immunostaining in adult WT and *Syn1-Cre;Mettl14*$^{f/f}$ cKO mice at SNL D3 (**D**; scale bar: 1 mm) and quantification (**E**). Values represent mean ± SEM (n = 6 animals; ****P* < 0.001; **P* < 0.05; two-way ANOVA).

(**F**) Immunostaining of cleaved-caspase 3 showing very low levels of cell death of DRG neurons at SNL D1. Scale bar: 200 μm.
(**G**) Sample images of skin nerve fibers stained with PGP9.5 from adult WT or AAV-Cre;*Mettl14* cKO mice at SNL D7 and with saphenous nerve ligation. Note that the SNL and saphenous nerve ligation resulted in complete denervation of axons in the footpad skin at SNL D7 for both WT and cKO animals. Scale bar: 20 μm.

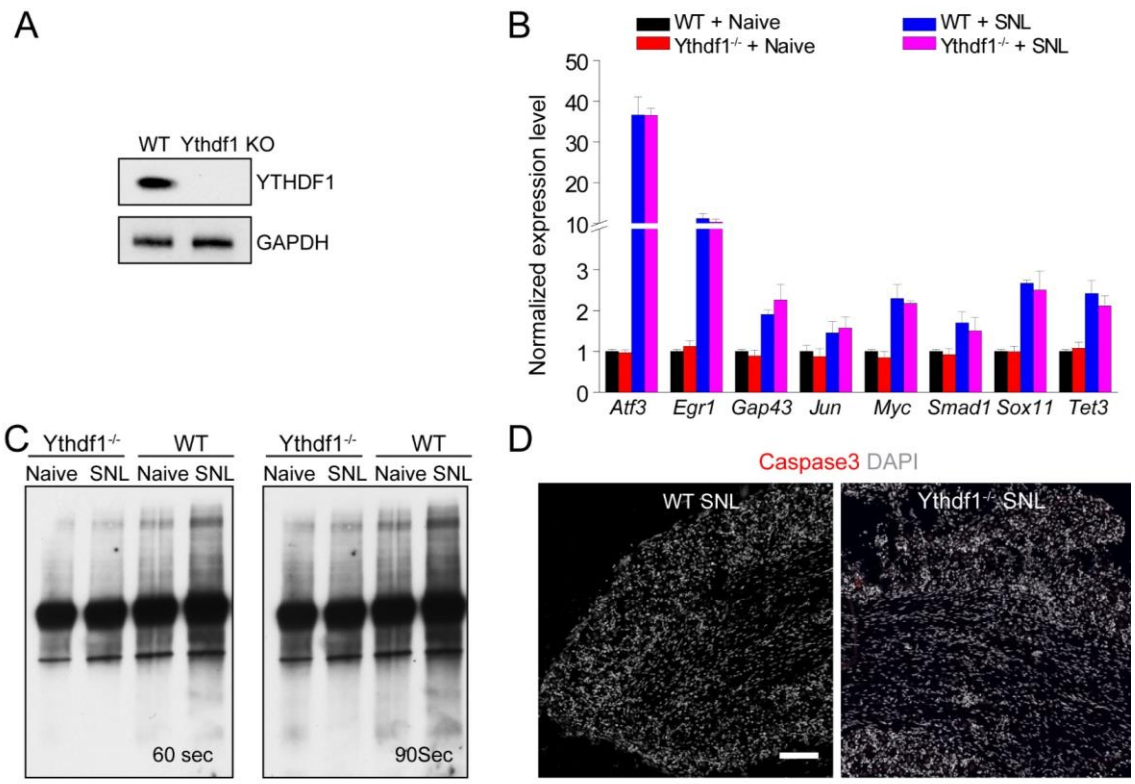


**Figure S5. *Ythdf1* knockout mice exhibited normal RAG induction, but defective de novo protein synthesis upon SNL, related to Figure 5.**

(**A**) Sample Western blot analysis of Ythdf1 expression in adult DRGs from WT and *Ythdf1* KO mice. GAPDH is shown as the loading control.
(**B**) Q-PCR analysis of mRNA levels for a selective group of RAGs in DRGs of WT and *Ythdf1* KO mice under naïve and SNL D1 conditions. Values represent ± SEM (n = 3 animals).
(**C**) SUnSET analysis of new protein synthesis in L4/5 DRGs of adult WT and *Ythdf1* KO mice. Same sample as in **Figure 5A**, but with different exposure times.
(**D**) Immunostaining of cleaved-caspase 3 showing very low levels of cell death of DRG neurons at SNL D1 in WT and *Ythdf1* KO mice. Scale bar: 200 μm.

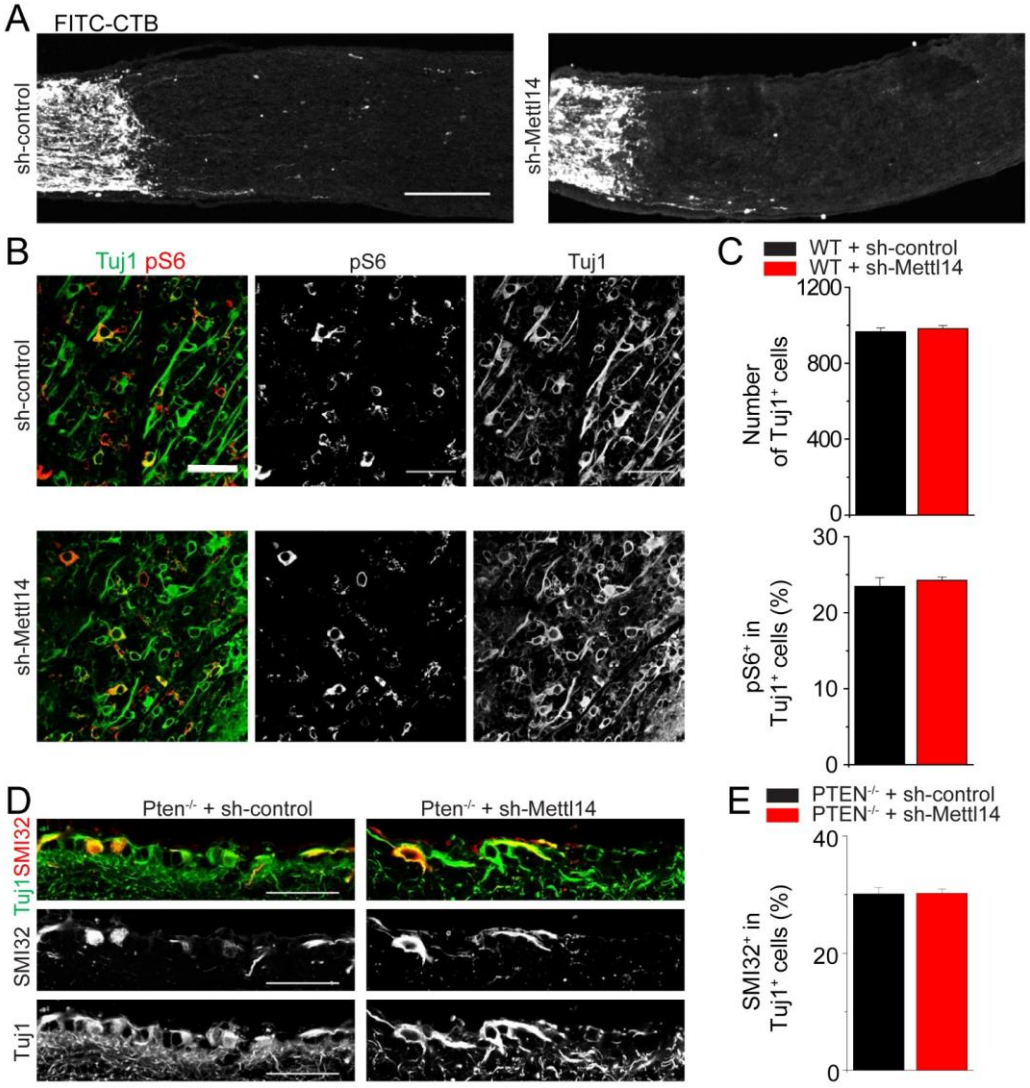


**Figure S6. Mettl14 is required for *Pten* deletion-induced axon regeneration of RGCs, related to Figure 6.**

(**A-C**) Adult WT mice were co-injected with AAV-Cre and AAV-control shRNA or AAV-Mettl14 shRNA. The optic nerve was crushed 4 weeks after AAV injection and RGC axons were traced by fluorescence conjugated cholera toxin B (FITC-CTB) 2 weeks later. Shown in (**A**) are sample images of sections of optic nerve containing CTB-labeled axons. Scale bar: 200 μm. Shown in (**B**) are sample images of whole-mount retina with Tuj1 (green) and pS6 (red) immunostaining. Scale bar: 50 μm. Shown in (**C**) are quantifications of densities of $Tuj1^+$ RGCs and percentages of $Tuj1^+$ RGCs expressing pS6. Values represent mean ± SEM (n = 5 animals).

(**D-E**) Adult *Pten*$^{f/f}$ mice were co-injected with AAV-Cre and AAV-control shRNA or AAV-Mettl14 shRNA, followed by optic nerve crush 4 weeks later and traced by FITC-CTB 2 weeks after crush. Shown in (**D**) are sample images of retina sections with Tuj1 (green) and SMI32 (red) immunostaining. Scale bar: 50 μm. Shown in (**E**) are quantifications of percentages of $Tuj1^+$ RGCs expressing SMI32. Values represent mean ± SEM (n = 5 animals).